

A mixed discontinuous/continuous finite element pair for shallow-water ocean modelling

Colin J. Cotter^{a,*} David A. Ham^b Christopher C. Pain^b

^a *Department of Aeronautics, Imperial College London, London SW7 2AZ, United Kingdom*

^b *Department of Earth Science and Engineering, Imperial College London, London SW7 2AZ, United Kingdom*

Abstract

We introduce a mixed discontinuous/continuous finite element pair for ocean modelling, with continuous quadratic layer thickness and discontinuous velocity. We investigate the finite element pair applied to the linear shallow-water equations on an f -plane. The element pair has the property that all geostrophically balanced states which strongly satisfy the boundary conditions have discrete divergence equal to exactly zero and hence are exactly steady states of the discretised equations. This means that the finite element pair has excellent geostrophic balance properties. We also show that the element pair applied to the non-rotating linear shallow-water equations does not have any spurious small eigenvalues. We illustrate these properties using numerical tests and provide convergence calculations which show that the numerical solutions have errors which decay quadratically with element edge length for both velocity and layer thickness.

1 Introduction

A number of finite element pairs have been proposed for the rotating shallow-water equations, including the $P1_{NC} - P1$ and $P1 - \text{iso } P2 - P1$ elements (investigated and compared to several other element pairs in (Le Roux et al., 1998)), the RT0 elements (introduced in Raviart and Thomas (1977) and

* Corresponding author.

Email addresses: colin.cotter@imperial.ac.uk (Colin J. Cotter), d.ham@imperial.ac.uk (David A. Ham), c.pain@imperial.ac.uk (Christopher C. Pain).

proposed for the shallow-water equations in Walters and Casulli (1998)) and equal-order elements with stabilisation (also proposed in Walters and Casulli (1998)); all of these elements have been shown to perform well when integrating the rotating shallow-water equations. In this paper we investigate the numerical properties of the $P1_{DG}$ - $P2$ finite element pair applied to the linear shallow-water equations on an f -plane in order to investigate the suitability of the element for shallow-water ocean modelling. The finite element pair consists of discontinuous linear elements for velocity and continuous quadratic elements for layer thickness. Even though the layer thickness has shape functions which are one order higher than velocity, there are still more degrees of freedom in the space of discontinuous linear functions than the space of continuous quadratic functions (except in meshes with very few elements), which is a necessary (but not sufficient) condition for the absence of spurious pressure modes (modes with high spatial frequency but small eigenvalues in the wave operator which can pollute the numerical solution with noise). In Cotter et al. (2008), it was shown that in one dimension, this choice leads to a discretisation of the wave equation without rotation which does not have any spurious modes. It was also shown that the dispersion relation is very accurate for the first half of the discrete spectrum. A number of numerical tests were carried out on two- and three-dimensional unstructured meshes which showed that there were no spurious eigenvalues present. In fact, as we show in this paper, the discretised Laplacian obtained by combining the first-order discrete divergence and gradient operators is the same as the usual Galerkin finite element discretised Laplacian obtained by multiplying the Laplacian by a test function and integrating by parts. Consequentially, the discretised equations without rotation do not have any spurious eigenvalues, also the element pair applied to the incompressible Navier-Stokes equations leads to an LBB-stable discretisation without spurious pressure modes. For a general discussion of LBB stability, see Gresho and Sani (2000); Karniadakis and Sherwin (2005). Karniadakis and Sherwin (2005) also contains an exposition of the discontinuous Galerkin method. For applications of the discontinuous Galerkin method to waves equations see Ainsworth et al. (2006), and for some applications of the discontinuous Galerkin method to the rotating shallow-water equations see Ambati and Bokhove (2007); Levin et al. (2006); Bernard et al. (2007); Giraldo (2006).

In this paper we concentrate on the interaction of the geostrophic modes with the inertia-gravity waves which is crucial to the good representation of large-scale dynamics. We find that not only does the finite element pair allow for accurate representation of geostrophically-balanced states, these states are completely uncoupled from the inertia-gravity waves: the states are exactly steady as in the unapproximated partial-differential equations. In section 2 we introduce the element pair applied to the linear shallow water equations, show that the element pair has a discrete Laplacian without spurious eigenvalues, and show that the element pair has exactly steady geostrophic states.

In section 3 we verify these results with numerical tests. We also show numerical calculations using Kelvin waves which are geostrophically balanced in one direction; these waves are a good test of preservation of balance. The results do not show any radiating inertia-gravity waves. We provide convergence test results using the Kelvin wave exact solution which confirm that the errors spatial discretisation converges quadratically for both velocity and layer thickness, indicating that the element pair is stable. Finally we give a summary and outlook in section 4.

2 The mixed element

In this section we describe our mixed element formulation applied to the linear shallow-water equations on an f -plane.

2.1 Mixed continuous/discontinuous Galerkin discretisation

We start with the linearised shallow-water equation on an f -plane in non-dimensional units

$$\mathbf{u}_t + \frac{1}{\text{Ro}} \mathbf{k} \times \mathbf{u} + \frac{1}{\text{Fr}^2} \nabla h = 0, \quad \mathbf{u} = (u_1, \dots, u_d), \quad (1)$$

$$h_t + \nabla \cdot \mathbf{u} = 0, \quad (2)$$

where \mathbf{u} is the velocity, h is the perturbation layer thickness, \mathbf{k} is the unit vector in the z -direction, $\text{Ro} = U/fL$ is the Rossby number, $\text{Fr} = \sqrt{U/gH}$ is the Froude number, U is a velocity scale, L is a horizontal length scale, H is the mean layer thickness, f is the Coriolis parameter and g is the acceleration due to gravity. The boundary conditions are

$$\mathbf{u} \cdot \mathbf{n} = 0 \quad \text{on} \quad \partial\Omega \quad (3)$$

where $\partial\Omega$ denotes the boundary of the domain Ω , and \mathbf{n} is the normal to $\partial\Omega$. To obtain the discontinuous/continuous Galerkin form of the equations we multiply equation (1) by a discontinuous test function \mathbf{w} and equation (2) by a continuous test function ϕ and integrate over an element E to obtain

$$\frac{d}{dt} \int_E \mathbf{w} \cdot \mathbf{u} \, dV + \frac{1}{\text{Ro}} \int_E \mathbf{w} \cdot \mathbf{k} \times \mathbf{u} \, dV = -\frac{1}{\text{Fr}^2} \int_E \mathbf{w} \cdot \nabla h \, dV, \quad (4)$$

$$\frac{d}{dt} \int_E \phi h \, dV = -\int_E \phi \nabla \cdot \mathbf{u} \, dV. \quad (5)$$

We then integrate equation (5) by parts, and make use of the boundary conditions (3) to obtain

$$\frac{d}{dt} \int_E \mathbf{w} \cdot \mathbf{u} \, dV + \frac{1}{\text{Ro}} \int_E \mathbf{w} \cdot \mathbf{k} \times \mathbf{u} \, dV = -\frac{1}{\text{Fr}^2} \int_E \mathbf{w} \cdot \nabla h \, dV, \quad (6)$$

$$\frac{d}{dt} \int_E \phi h \, dV = \int_E \nabla \phi \cdot \mathbf{u} \, dV \quad (7)$$

$$- \int_{\partial E \setminus \partial \Omega} \mathbf{n} \cdot \tilde{\mathbf{u}} \phi \, dS, \quad (8)$$

where $\tilde{\mathbf{u}}$ is the value of \mathbf{u} on the element boundary ∂E , determined by the particular choice of discontinuous Galerkin scheme which is chosen (the value on the upwind face, for example), and where \mathbf{n} is the outward-pointing unit normal to the surface ∂E . Conservation requires that $\tilde{\mathbf{u}}$ takes the same value on either side of each face. We sum these equations over all elements and the surface terms cancel since ϕ is continuous. This gives the form of the equations that we will discretise:

$$\frac{d}{dt} \int_{\Omega} \mathbf{w} \cdot \mathbf{u} \, dV + \frac{1}{\text{Ro}} \int_{\Omega} \mathbf{w} \cdot \mathbf{k} \times \mathbf{u} \, dV = -\frac{1}{\text{Fr}^2} \int_{\Omega} \mathbf{w} \cdot \nabla h \, dV, \quad (9)$$

$$\frac{d}{dt} \int_{\Omega} \phi h \, dV = \int_{\Omega} \nabla \phi \cdot \mathbf{u} \, dV. \quad (10)$$

Derivatives are only applied to the scalar functions h and ϕ and not the vector functions \mathbf{u} and \mathbf{w} which we shall discretise with discontinuous elements. To add nonlinear advection it is necessary to develop surface integrals on the boundaries of the elements following the standard discontinuous Galerkin finite element approach.

2.2 The $P1_{DG}$ - $P2$ element

In this subsection we develop the $P1_{DG}$ - $P2$ discretisation for the shallow-water equations. We make the choice that \mathbf{u} and \mathbf{w} are approximated by discontinuous linear finite element functions \mathbf{u}^δ and \mathbf{w}^δ , whilst ϕ and h are approximated by continuous quadratic linear finite element functions h^δ and ϕ^δ .

The Galerkin finite element approximation of equations (9,10) is then

$$\frac{d}{dt} \int_{\Omega} \mathbf{w}^\delta \cdot \mathbf{u}^\delta \, dV + \frac{1}{\text{Ro}} \int_{\Omega} \mathbf{w}^\delta \cdot \mathbf{k} \times \mathbf{u}^\delta \, dV = -\frac{1}{\text{Fr}^2} \int_{\Omega} \mathbf{w}^\delta \cdot \nabla h^\delta \, dV,$$

$$\frac{d}{dt} \int_{\Omega} \phi^\delta h^\delta \, dV = \int_{\Omega} \nabla \phi^\delta \cdot \mathbf{u}^\delta \, dV,$$

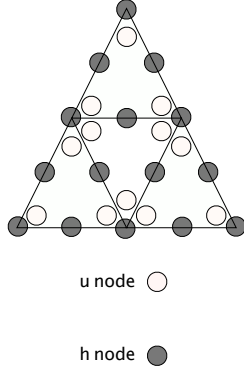


Fig. 1. Figure showing the distribution of nodes in the two-dimensional $P1_{DG}$ - $P2$ element. Each element contains three nodes for each of the two components u and v of velocity, and six nodes for the layer thickness, but the latter nodes are shared across element boundaries since the layer thickness space is continuous.

for all test functions ϕ^δ and \mathbf{w}^δ in the specified spaces.

2.3 Properties of discretised Laplacian

The first property to note for the $P1_{DG}$ - $P2$ element pair is that the discretised gradient in the $P1_{DG}$ velocity space \mathbf{q}^δ of a $P2$ function h^δ obtained from

$$\int_{\Omega} \mathbf{w}^\delta \cdot \mathbf{q}^\delta \, dV = \int_{\Omega} \mathbf{w}^\delta \cdot \nabla h^\delta \, dV$$

for all $P1_{DG}$ test functions \mathbf{w}^δ , satisfies

$$\mathbf{q}^\delta = \nabla h^\delta$$

at each point. To prove this, note that all continuous $P2$ functions h have $P1_{DG}$ gradients. This means that we may choose $\mathbf{w}^\delta = \mathbf{q}^\delta - \nabla h^\delta$ and hence

$$\int_{\Omega} |\mathbf{q}^\delta - \nabla h^\delta|^2 \, dV = 0.$$

Since \mathbf{q}^δ and ∇h^δ are piecewise polynomials this means that they are identically equal.

The discretised Laplacian L^δ in the layer thickness space is obtained by applying the discretised divergence to the discretised gradient \mathbf{q}^δ :

$$\begin{aligned} \int_{\Omega} \phi^{\delta} L^{\delta} h^{\delta} \, dV &= - \int_{\Omega} \nabla \phi^{\delta} \cdot \mathbf{q}^{\delta} \, dV + \int_{\partial\Omega} \phi^{\delta} \vec{n} \cdot \mathbf{q}^{\delta} \, dS \\ &= - \int_{\Omega} \nabla \phi^{\delta} \cdot \nabla h^{\delta} \, dV + \int_{\partial\Omega} \phi^{\delta} \frac{\partial h^{\delta}}{\partial n} \, dS, \end{aligned}$$

for any $P2$ test function ϕ^{δ} , which is the standard Galerkin finite element discretisation of the Laplace operator obtained by multiplying by a test function and integrating by parts. The properties of this operator are well-known in the finite element literature; in particular it has no spurious eigenvalues.

2.4 Exactly steady geostrophic modes

In the linear shallow-water equations with rotation, the geostrophic balanced modes with

$$\mathbf{u}_t = 0 \implies \mathbf{u} = \nabla^{\perp} \psi, \quad (11)$$

are steady in time, where

$$\psi = \frac{\text{Ro}}{\text{Fr}^2} h, \quad \nabla^{\perp} \psi = (-\psi_y, \psi_x)$$

This is because $h_t = 0$ since $\nabla \cdot \mathbf{u} = 0$ for these modes. In this section we show that the balanced states in discretisations with the $P1_{\text{DG}}\text{-}P2$ element pair are also completely steady; this means that the $P1_{\text{DG}}\text{-}P2$ element pair represents balanced states very well and so is ideal for shallow-water ocean modelling.

The geostrophically balanced states in the finite element discretisation satisfy

$$\frac{d}{dt} \int_{\Omega} \mathbf{w}^{\delta} \cdot \mathbf{u}^{\delta} \, dV = 0, \quad \implies \int_{\Omega} \mathbf{w}^{\delta} \cdot \mathbf{u}^{\delta} \, dV = \int_{\Omega} \mathbf{w}^{\delta} \cdot \nabla^{\perp} \psi^{\delta} \, dV, \quad (12)$$

for all $P1^{DG}$ test functions \mathbf{w}^{δ} .

The property described in the previous section can be trivially extended to show that the finite element velocity \mathbf{u}^{δ} obtained from this equation for a given ψ^{δ} satisfies equation (11) with $u = u^{\delta}$ and $\psi = \psi^{\delta}$. We can use this property to show that any geostrophically balanced velocity field \mathbf{u} obtained from a streamfunction ψ which is constant on the boundary satisfies the discrete divergence equation

$$- \int_{\Omega} \nabla \phi^{\delta} \cdot \mathbf{u}^{\delta} \, dV = 0,$$

for all $P2$ test functions ϕ^{δ} . To prove this, note that

$$-\int_{\Omega} \nabla \phi^{\delta} \cdot \mathbf{u}^{\delta} \, dV = -\int_{\Omega} \nabla \phi^{\delta} \cdot \nabla^{\perp} \psi^{\delta} \, dV \quad (13)$$

$$= \sum_E \int_E \phi^{\delta} \underbrace{\nabla \cdot \nabla^{\perp} \psi^{\delta}}_{=0} \, dV - \sum_E \int_{\partial E} \phi^{\delta} \mathbf{n} \cdot \nabla^{\perp} \psi^{\delta} \, dS \quad (14)$$

$$= -\sum_{\Gamma} \int_{\Gamma} \phi^{\delta} \underbrace{[[\mathbf{n} \cdot \nabla^{\perp} \psi^{\delta}]]}_{=0} \, dV - \int_{\partial\Omega} \phi^{\delta} \underbrace{\mathbf{u} \cdot \mathbf{n}}_{=0} \, dS = 0 \quad (15)$$

where \sum_E indicates a sum over all elements E , ∂E is the boundary of element E , \sum_{Γ} indicates a sum over all orientated internal element boundaries in the mesh, and $[[f]]$ indicates the jump in a function f across a surface Γ . In equation (14) the normal component of velocity vanishes exactly on $\partial\Omega$ as h is constant on $\partial\Omega$ and the balanced velocity is obtained from the pointwise curl of the streamfunction ψ . In (15) the jump in the normal component of $\nabla^{\perp} \psi$ vanishes because the tangential derivative of functions in $P2$ is continuous across element boundaries.¹

The proof of this property is easily extended to the general $P_{n_{DG}}-P_{(n+1)}$ element pair i.e., n th order discontinuous velocity and $(n+1)$ -th order continuous layer thickness. It is also easily extended to the three-dimensional case in which $\mathbf{u} = \nabla \wedge \Psi$ for any vector field Ψ which is constant on the boundary.

3 Numerical tests

In this section we illustrate and explore the properties of the $P1_{DG}-P2$ element applied to the linear rotating shallow-water equations.

3.1 Representation of geostrophic balance

Le Roux et al. (1998) tested a number of element pairs for their ability to represent geostrophic balance. This was done by selecting a streamfunction field, computing the balanced velocity field from equation (12), and plotting streamlines. Element pairs were compared by the smoothness of the resulting streamlines on structured and unstructured meshes. Here we just note that, as described in the previous section, the balanced velocity for the $P1_{DG}-P2$ element is obtained from the pointwise gradients of streamfunction and so streamlines of the discretised balanced velocity field are simply contours of

¹ The right-hand side of (13) can be shown to vanish for general functions from the space H^1 (which contains the $P2$ functions) by taking a convergent sequence of smooth functions and passing to the limit. However, the extra property of continuous tangential derivatives of Pn functions facilitates the simpler proof given here.

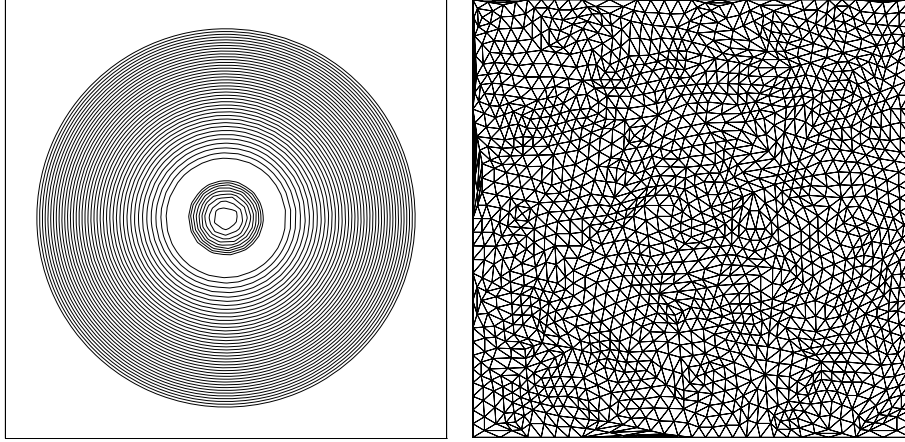


Fig. 2. **Left:** Streamlines of balanced velocity obtained from a Gaussian streamfunction distribution using the $P1_{DG}$ - $P2$ discretisation. The streamlines are very smooth showing that the discretisation does not introduce spurious oscillations. This is because in this case the balanced velocity can be obtained by taking the pointwise (strong) gradients of the streamfunction. **Right:** The mesh used for this calculation. The mesh was deliberately distorted to illustrate that this property is not dependent on mesh quality.

the discretised streamfunction field. This means that the balanced velocity field is actually as accurate as possible for the $P2$ streamfunction field. Plots of some resulting streamlines are given in figure 2; for comparison with other element pairs see Le Roux et al. (1998).

3.2 Steady states

In Le Roux et al. (1998), another numerical test was performed in which the linear rotating shallow-water equations were initialised in a geostrophic state; streamlines were plotted after some time which showed that the $P1$ iso $P2-P0-3$ element pair (proposed in that paper) preserved the steady state to excellent accuracy. In the case of the $P1_{DG}$ - $P2$ element, we have already shown in the previous section that geostrophic states are exactly steady so it remains to verify this numerically. Using the mesh shown in figure 2, we computed randomly generated streamfunction fields with $\psi = 0$ on the boundary together with their geostrophically balanced velocity fields obtained from equation (11), and integrated the equations in time using the Crank-Nicholson method. We observed that the layer thickness h and velocity \mathbf{u} remained constant up to machine precision, confirming that the geostrophic modes are completely uncoupled from the inertia-gravity waves. For the time evolution of geostrophic states using other element pairs, see Le Roux et al. (1998).

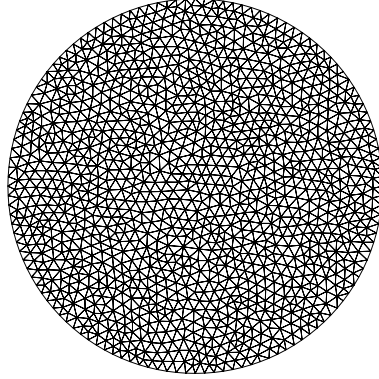


Fig. 3. Plot showing the mesh used for Kelvin wave tests.

3.3 Kelvin waves

We tested the $P1_{DG}$ - $P2$ element using a Kelvin wave initial condition; the Kelvin wave is a trapped coastal wave which is geostrophically balanced in the direction normal to the coast which propagates at the fast gravity wave speed $1/\text{Fr}$ for the case of a straight coastline. The aim of the test is to verify that the Kelvin wave does not shed any spurious inertia-gravity waves. We used the circular Kelvin wave initial condition given by

$$\begin{aligned} h(r, \theta) &= e^{(r-r_0)/\text{Ro}} \cos \theta, \\ u_\theta(r, \theta) &= \frac{1}{\text{Fr}} e^{(r-r_0)/\text{Ro}} \cos \theta, \\ u_r &= 0, \end{aligned}$$

with $\text{Ro} = 0.1$ and $\text{Fr} = 1$. The Kelvin wave propagates around the circular coast, maintaining geostrophic balance in the normal direction. The mesh used for the discretisation is shown in figure 3. We integrated the equations in time for $0 > t > 100$ using the Crank-Nicholson method and a time step size $\Delta t = 0.01$. Figure 4 shows the layer thickness at various times: there are no spurious gravity waves observed, which means that the $P1_{DG}$ - $P2$ element pair is maintaining geostrophic balance in the normal direction as well as the Kelvin wave structure.

To check convergence of the method we integrated a Kelvin wave in the rectangular domain $\Omega = \{\mathbf{x} : -15 < x < 15, 0 < y < 3\}$ with initial condition

$$h = e^{-y/\text{Ro}} e^{-(x-5)^2}, \quad \mathbf{u} = (e^{-y/\text{Ro}} e^{-(x-5)^2}, 0).$$

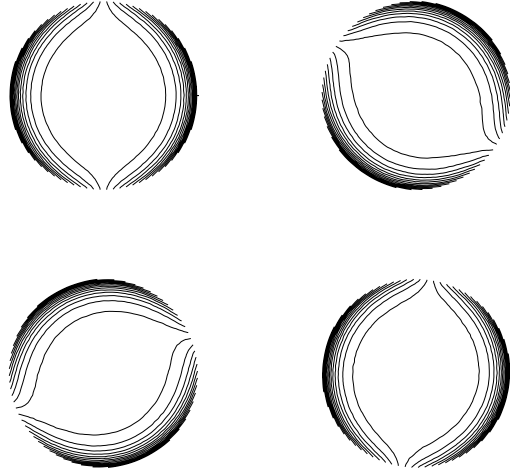


Fig. 4. Plots showing contours of layer thickness h at times $t = 0$ (top left), 30 (top right), 60 (bottom left) and 90 (bottom right) for the circular Kelvin wave test case. No spurious oscillations are observed, which verifies that the $P1_{DG}$ - $P2$ element maintains geostrophic balance in the normal direction.

If this initial condition is used in the domain $\Omega^\infty = \{\mathbf{x} : -\infty < x < \infty, 0 < y < \infty\}$, then the equation has the exact solution

$$h = e^{-y/\text{Ro}} e^{-(x+t/\text{Fr}^2-5)^2}, \quad \mathbf{u} = (e^{-y/\text{Ro}} e^{-(x+t/\text{Fr}^2-5)^2}, 0).$$

We integrated the system to time $t = 10$. For this time interval the solution is almost zero for $y > 1$ and $|x| > 6$ and so the exact solution is a good approximation. The timestep was chosen to have a wave Courant number of less than 0.1 for all simulations so that the errors are dominated by the spatial discretisation. We refined the mesh isotropically in space in the region where the solution was non-zero during the calculation and computed the L_2 errors of the velocity and the layer thickness for various element edge lengths in the refined region. Plots of the numerical errors are given in figure 5. A linear regression on these values showed that the velocity errors were proportional to 2.19 and the layer thickness errors were proportional to 1.98. These results suggest that the errors in velocity and layer thickness in the spatial discretisation scale quadratically with the edge length, as would be expected from approximation theory. They are also an indication that the element pair is stable: if the element pair were unstable then there would be spurious modes present which would lead to slower convergence than that expected from approximation theory.

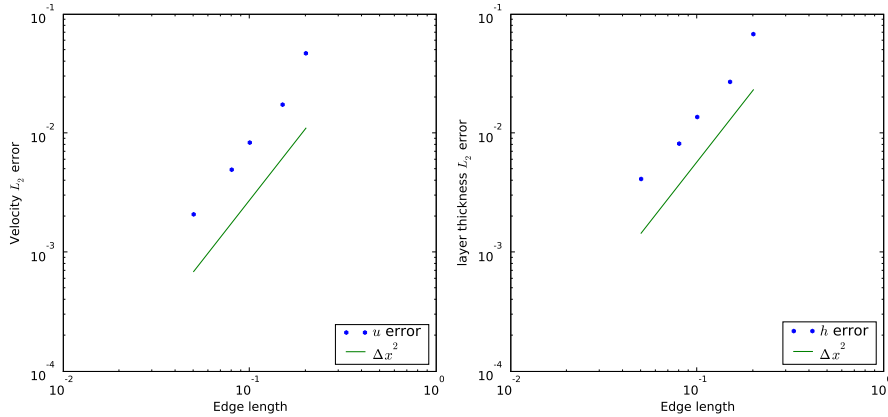


Fig. 5. Convergence plots for tests with a Kelvin wave propagating along a flat coast performed on unstructured isotropic triangular meshes, showing error ϵ against element edge length Δx . **Left:** L_2 error in velocity plotted against element edge length. **Right:** L_2 error in velocity plotted against element edge length. Both plots show that the errors scale with Δx^2 as $\Delta x \rightarrow 0$.

4 Summary and Outlook

In this paper we introduced the $P1_{DG}$ - $P2$ element pair applied to the linear shallow-water equations on an f -plane. We showed that the element pair has the property that all geostrophically balanced states which strongly satisfy the boundary conditions are exactly steady since their discrete divergence is identically zero. This means that the element pair has excellent geostrophic balance properties. We verified these properties by computing the evolution of balanced states, and by simulating Kelvin wave solutions which are geostrophically balanced in one direction. Finally we gave convergence test results which show that the numerical solutions have errors which decay quadratically with element edge length; this verifies the LBB-stability properties discussed in Cotter et al. (2008).

In future work we shall compare this element pair with other low-order element pairs such as the $P0_{DG} - P1$, $P1_{NC} - P1$ and $RT0$ pairs. Whilst the discontinuous velocity means that the $P1_{DG}$ - $P2$ pair has a large number of degrees of freedom per element, the remarkable accuracy of the first half of the dispersion relation (noted in Cotter et al., 2008) suggests that the element may be competitive, especially given its excellent treatment of geostrophic balance, and local conservation of momentum. The higher-order extensions such as $P2_{DG} - P3$ will also be examined. We shall investigate the performance of the element once nonlinear advection has been introduced.

A key advantage of this element pair is that the extension to three dimensions is also LBB-stable; the property that geostrophically balanced states are exactly divergence-free also extends to the three dimensional case. We shall

investigate the performance of this element pair in fully three-dimensional unstructured mesh ocean modelling in the ICOM model (Pain et al., 2005). We also expect that if the buoyancy is discretised using $P1_{DG}$ elements, then the discretisation will also preserve hydrostatic balance very well; this will be investigated in future work.

5 Acknowledgements

We thank Greg Pavliotis for discussions about the proof that the geostrophic modes are completely decoupled for this element pair, and all of the AMCG team for their collaborative contributions. The authors acknowledge funding from NERC consortium grant NE/C52101X/1.

References

- Ainsworth, M., Monk, P., Muniz, W., 2006. Dispersive and dissipative properties of discontinuous Galerkin finite element methods for the second-order wave equation. *J. Sci. Comput.* 27 (1-3), 5–40.
- Ambati, V., Bokhove, O., 2007. Space-time discontinuous galerkin discretization of rotating shallow water equations. *Journal of Computational Physics* 225 (2), 1233–1261.
- Bernard, P. E., Chevaugeon, N., Legat, V., Deleersnijder, E., Remacle, J. F., 2007. High-order h-adaptive discontinuous galerkin methods for ocean modelling. *Ocean Dynamics* 57, 109–121.
- Cotter, C. J., Ham, D. A., Pain, C. C., Reich, S., 2008. LBB stability of a mixed Galerkin finite element pair, submitted <http://arxiv.org/0707.4607>.
- Giraldo, F. X., 2006. High-order triangle-based discontinuous galerkin methods for hyperbolic equations on a rotating sphere. *J. Comput. Phys.* 214 (2), 447–465.
- Gresho, P. M., Sani, R. L., 2000. *Incompressible Flow and the Finite Element Method, Volume 2, Isothermal Laminar Flow*. Wiley.
- Karniadakis, G. E. M., Sherwin, S., 2005. *Spectral/hp Element Methods for Computational Fluid Dynamics*. Oxford Science Publications, Ch. 7.
- Le Roux, D., Staniforth, A., Lin, C. A., 1998. Finite elements for shallow-water equation ocean models. *Monthly Weather Review* 126 (7), 1931–1951.
- Levin, J., Iskandarani, M., Haidvogel, D., 2006. To continue or discontinue: Comparisons of continuous and discontinuous Galerkin formulations in a spectral element ocean model. *Ocean Modelling* 15, 56–70.
- Pain, C., Piggott, M., Goddard, A., Fang, F., Gorman, G., Marshall, D., Eaton, M., Power, P., de Oliveira, C., 2005. Three-dimensional unstructured mesh ocean modelling. *Ocean Modelling* 10, 5–33.

- Raviart, Thomas, 1977. A mixed finite element method for 2nd order elliptic problems. In: *Mathematical Aspects of the Finite Element Method*. Lecture Notes in Mathematics. Springer, Berlin.
- Walters, R., Casulli, V., 1998. A robust, finite element model for hydrostatic surface water flows. *Communications in Numerical Methods in Engineering* 14, 931–940.